

A Piecewise Linear Suspension Bridge Model: Nonlinear Dynamics and Orbit Continuation

S. H. Doole
Department of Engineering Mathematics
Bristol University
Queen's Building, University Walk
Bristol U. K. BS8 1TR
`stuart.doole@bristol.ac.uk`

S. J. Hogan
Department of Engineering Mathematics
Bristol University
Queen's Building
University Walk
Bristol U. K. BS8 1TR
`s.j.hogan@bristol.ac.uk`

To appear:
Dynamics and Stability of Systems **11**(1), 1996

Running title:
Nonlinear Dynamics of Suspension Bridges

A Piecewise Linear Suspension Bridge Model: Nonlinear Dynamics and Orbit Continuation.

S. H. Doole and S. J. Hogan

Abstract

The effect of harmonic excitation on suspension bridges is examined as a first step towards the understanding of wind, and possibly certain kinds of earthquake, excitation upon such structures. The Lazer-McKenna suspension bridge model is studied completely for the first time by using a methodology which has been successfully applied to models of rocking blocks and other free-standing rigid structures. An unexpectedly rich dynamical structure is revealed in this way. Conditions for the existence of asymptotic periodic responses are established, via a complicated nonlinear transcendental equation. A two part Poincaré map is derived to study the orbital stability of such solutions. Numerical results are presented which illustrate the application of the analytical procedure to find and classify stable and unstable solutions; as well as determine bifurcation points accurately. The richness of the possible dynamics is then illustrated by a menagerie of solutions which exhibit fold and flip bifurcations, period doubling, period adding and sub/super-harmonic coexistence of solutions. The solutions are shown both in the phaseplane, and as Poincaré map fixed points under parameter continuation using the package AUTO. Such results illustrate the possibility of the coexistence of ‘dangerous’ large amplitude responses at the same point of parameter space as ‘safe’ solutions. The feasibility of experimental verification of the results is discussed.

KEYWORDS: suspension bridges, Lazer-McKenna model, nonlinear dynamics, Poincaré maps, subharmonic orbits, AUTO continuation, piecewise linear ODEs.

1 Introduction

In this paper, we consider the effect of harmonic excitation on suspension bridges as a first stage towards the understanding of the action of wind (and perhaps certain kinds of earthquake) upon such structures. In particular, our interest lies in the role of the one sided stiffness of the hangers (between roadbed and cable) in the resultant transverse and torsional motions. One source of motivation was the work of Lazer & McKenna and others (Lazer & McKenna 1987, Glover, Lazer & McKenna 1989, Lazer & McKenna 1990, Lazer & McKenna 1991, Choi, Jen & McKenna 1991, Jacover & McKenna 1994) on the modelling of suspension bridges. They consider the bridge deck to be a one-dimensional vibrating beam of length L connected to the main suspension cable by stays and hinged at each end. The stays are treated as one-sided springs. That is, they are assumed to provide a linear restoring force if stretched but to offer no resistance to compression. If deflection of the main cable is neglected, the following (scaled) equation for the downward deflection $u(x, t)$ of the bridge deck is obtained

$$u_{tt} + u_{xxxx} = -pu_t - ku^+ + W(x) + F(x, t), \quad (1.1)$$

with the hinged boundary conditions

$$u(0, t) = u(L, t) = u_{xx}(0, t) = u_{xx}(L, t) = 0. \quad (1.2)$$

(We will describe our preferred scaling in § 2.) The righthand side of (1.1) includes the (small) wind resistance term pu_t , k as the spring constant ($u^+ := \max\{u, 0\}$), $W(x)$ as the weight per unit length and $F(x, t)$ as the forcing term. Lazer & McKenna (Lazer & McKenna 1990) introduce the one-sided spring as a nonlinear mechanism which may account for such wind related disasters as the collapse of the bridge at Tacoma Narrows in 1940 (Bleich, McCullough, Rosecrans & Vincent 1950, Farquharson 1950). We shall show (amongst other things) that large amplitude subharmonic responses can occur for small amplitude excitations across open intervals of parameter values. This ‘broad band’ mechanism for bridge collapse seems more plausible than one based on resonance. This latter explanation has no longer any currency within the engineering community either (Billah & Scanlan 1991), but opinion remains strongly divided as to the details of any replacement (Peterson 1990, Petroski 1991, McKenna 1992). Scanlan and co-workers (Billah & Scanlan 1991) prefer to note which mode appears to lose stability to the torsional motion and then pose a two degree of freedom oscillator, whose coefficients are matched with certain experimental or field measurements. It may be, that in future studies, such an oscillator will be derivable via centre manifold/amplitude equation techniques as the appropriate low dimensional model. In the meantime, there exists no *explicit* mechanism for the transitions between essentially one and two dimensional motions, or the reductions of the full dynamics to the postulated oscillator.

We use a similar model to (Lazer & McKenna 1990) but provide the first complete analysis of this work by applying the machinery developed by Hogan (Hogan 1989, Hogan 1990, Hogan 1992*a*, Hogan 1992*b*, Hogan 1994) to the analysis of piecewise linear ODEs arising from (1.1-1.2) via separation of the variables. This approach reveals, for the first time, a rich dynamical structure which will prove valuable in further studies. Such a model is a plausible first step on the road to understanding *systematically* the large scale oscillations of a bridge like the Tacoma Narrows and the loss of stability to a torsional mode. Clearly the one-sided spring effect is highly important in bridges undergoing *torsion* and this two-dimensionality will be incorporated in future work. However, until the simplest asymmetric model is better understood, it seems over-ambitious to study a ‘more physical’ case. Moreover, the solutions obtained and understood in the one dimensional model will be used as a basis for accurate continuation in a model including torsion, in order to the yield explicit paths in parameter space between torsional and vertical motions, which are the ultimate aim of this work.

Conditions for the existence of asymptotic periodic responses to the piecewise linear ODE model are established in § 3 and 4. The first set is for simple preloaded orbits; and the second, for full phase-space orbits, involves the derivation of a complicated nonlinear transcendental equation. A two part Poincaré map is derived to study the orbital stability of the latter class of solutions. Numerical results are presented which illustrate the application of the analytical procedure to find and classify stable and unstable solutions, as well as determine bifurcation points accurately. The richness of the possible dynamics is shown by a menagerie of solutions which show fold

and flip bifurcations, period doubling, period adding and sub/super-harmonic coexistence of solutions. This is done by a combination of direct simulation of the ODEs and parameter continuation of fixed points of an appropriate Poincaré map. The possibility of experimental verification of these results is also discussed.

2 The Piecewise Linear ODE and its Scaling

As has been described, the bridge is modelled by a beam with hinged end boundary conditions. The full, dimensional field equation is (Timoshenko 1928, Thomson 1993)

$$Mu_{tt} + EIu_{xxxx} + \delta'u_t = -k'u^+ + W(x) + F(x, t), \quad (2.1)$$

where $u > 0$ is downwards deflection, M is the mass per unit length, EI the flexural rigidity (that is, the product of the beam's Young's modulus and the second moment of the cross-sectional area), δ' is viscous/wind damping, k' is the Young's modulus of the stay, W is the weight distribution and F is the external forcing. The boundary conditions are given by equation (1.2). Equation (2.1) is first simplified by the 'no-node' approximation. That is,

$$F(x, t) = B' \sin \omega' t \sin \frac{\pi x}{L}, \quad W(x) = W' \sin \frac{L}{\pi}. \quad (2.2)$$

Certainly, it is reasonable for a first approach to the problem to consider just this basic mode. Moreover, Scanlan (Billah & Scanlan 1991) describes how for the Tacoma Narrows Bridge disaster, it was this mode that apparently first lost stability to torsional oscillations. See also (Glover et al. 1989, Lazer & McKenna 1990). Next we separate variables as follows

$$u(x, t) = y(t) \sin \frac{\pi x}{L}, \quad (2.3)$$

where $y > 0$ is deflection downwards. The natural scalings of time and length

$$\hat{t} = \left(\frac{EI}{M} \right)^{1/2} t, \quad \hat{x} = \left(\frac{\pi}{L} \right) x. \quad (2.4)$$

are then introduced. These differ from those chosen in (Lazer & McKenna 1990) since we have scaled L out of the problem in order to isolate those dynamics associated with the hanger stiffness asymmetry. It also removes the singular behaviour which would occur if L was increased appreciably beyond π . The use of scaling (2.4) allows the geometric comparison of numerically computed orbits and the direct physical interpretation of numerical results in terms of the type of suspension bridge being modelled. For this reason, we use these 'physical' parameters in §6. Dropping hats, we obtain the transformed equations

$$\begin{aligned} y'' + 2\delta y' + (k + 1)y &= W + B \sin \omega t, & y > 0, \\ y'' + 2\delta y' + y &= W + B \sin \omega t, & y < 0, \end{aligned} \quad (2.5)$$

where the prime denotes differentiation with respect to t , and the nondimensional constants are defined by

$$\delta = \frac{\delta'}{2\sqrt{EIM}}, \quad k = \frac{k'}{EI}, \quad \omega = \omega' \left(\frac{M}{EI} \right)^{1/2}, \quad W = \frac{W'}{EI}, \quad B = \frac{B'}{EI}. \quad (2.6)$$

Equations (2.5) are, of course, similar to those that have been studied in the impact oscillator literature by, for example, Shaw (Shaw & Holmes 1983, Shaw 1985*a*, Shaw 1985*b*), Thompson (Thompson, Bokian & Ghaffari 1983), Whiston (Whiston 1987*a*, Whiston 1987*b*, Whiston 1992) Hogan (Hogan 1989), Budd (Budd, Dux & Cliffe 1993, Budd & Dux 1994) Nordmark (Nordmark 1991, Stensson & Nordmark 1994) and many others. (See also the special issue of *Phil. Trans. Roy. Soc.*, edited by (Bishop 1994), for a wide range of the current theoretical and experimental work in the area.) The basic techniques developed for the treatment of those piecewise linear ordinary differential equations are applied here. However, the nonzero preload W cannot be removed by simple translation, for example, and we stress that equations (2.5) do not reduce to any previously published case. Consequently, we include some details of the analysis. To organise efficiently the solutions obtainable by direct computation, and to make any numerical search more effective, we begin by studying simple (asymptotic) periodic responses analytically. Then we consider the stability of these solutions. In this way, other asymptotic trajectories can be classified and realized as the result of bifurcations from the simple periodic orbits. Note, too, that because of the physical scenario we are modelling, it is periodic orbits rather than chaotic ones that are of interest.

For simplicity in the subsequent analysis, we introduce the parameters $F = B/W$ and $m = k + 1 > 1$ and scale $W\hat{y} = y$. We proceed to solve first for $\hat{y} > 0$. We define $\hat{z}(t) = \hat{y}'(t)$ and denote the solutions in this half of phase space by the $+$ subscript. Initial conditions at a time t_o are also imposed, namely

$$\hat{y}_+(t_o) = y_o, \quad \hat{z}_+(t_o) = z_o. \quad (2.7)$$

The explicit solutions to governing equations are then given by

$$\begin{aligned} \hat{y}_+(t) &= \frac{1}{m} + \gamma \sin \omega t + \chi \cos \omega t + e^{\delta(t_o-t)} \left(\left(y_o - \frac{1}{m} - \gamma s_o - \chi c_o \right) \cos \sqrt{m - \delta^2}(t - t_o) \right. \\ &\quad \left. + (\delta y_o + z_o - \frac{\delta}{m} + \beta s_o - \alpha c_o)(m - \delta^2)^{-1/2} \sin \sqrt{m - \delta^2}(t - t_o) \right), \\ \hat{z}_+(t) &= \gamma \omega \cos \omega t - \chi \omega \sin \omega t + e^{\delta(t_o-t)} \left((z_o - \gamma \omega c_o + \chi \omega s_o) \cos \sqrt{m - \delta^2}(t - t_o) \right. \\ &\quad \left. + (1 - \delta z_o - m y_o + \lambda s_o + \omega \beta c_o)(m - \delta^2)^{-1/2} \sin \sqrt{m - \delta^2}(t - t_o) \right). \end{aligned} \quad (2.8)$$

where $c_o = \cos \omega t_o$, $s_o = \sin \omega t_o$, and the other parameters are defined by

$$\begin{aligned} \gamma &= \frac{F(m - \omega^2)}{(m - \omega^2)^2 + (2\omega\delta)^2}, & \chi &= -\frac{2\omega\delta F}{(m - \omega^2)^2 + (2\omega\delta)^2}, \\ \alpha &= \frac{F\omega(m - 2\delta^2 - \omega^2)}{(m - \omega^2)^2 + (2\omega\delta)^2}, & \beta &= -\frac{F\delta(m + \omega^2)}{(m - \omega^2)^2 + (2\omega\delta)^2}, \\ \lambda &= \frac{F(m^2 - \omega^2 m + 2(\omega\delta)^2)}{(m - \omega^2)^2 + (2\omega\delta)^2}. \end{aligned} \quad (2.9)$$

The solutions for $\hat{y} < 0$, denoted \hat{y}_- , \hat{z}_- respectively, can be obtained from (2.8) by setting $m = 1$ in all expressions and replacing instances of t_o by t_1 , z_o by z_1 , c_o by c_1 and s_o by s_1 .

In the sequel, we will discuss a range of solutions and their bifurcations, and it is appropriate to introduce a classification scheme for these orbits. Following (Hogan 1989), we call a periodic asymptotic response an (ℓ, n) -solution if the trajectory passes the positive z -axis ℓ times before the motion repeats, *and* that during that motion, n periods of forcing occur. This notation is closely related to the two types of Poincaré map that we will use. There is the stroboscopic map \mathcal{S} defined in the phaseplane for a fixed *phase* which acts on the position and velocity. Alternatively, there is the ‘impact’ map P , which maps the phase and velocity upon intersection with $\{y = 0, z > 0\}$. That is, one records the phase and velocity as the beam passes through the rest state downwards. Both have their advantages. The stroboscopic map is easy to define globally and is a well understood tool in nonlinear oscillator problems. There are technical difficulties in making the impact map well-defined, but it is better for understanding bifurcations such as *grazes* which do not occur in smooth dynamical systems. Such issues are discussed in much greater detail in (Whiston 1987*a*, Whiston 1992, Foale & Bishop 1992, Nordmark 1991, Nordmark 1992, Budd 1993). Thus an (ℓ, n) -orbit is a fixed point of P^ℓ and \mathcal{S}^n .

3 Existence of Preloaded Orbits

The first type of asymptotic response we analyse consists of those orbits which lie in only one half of the phaseplane. (Simple phase plane arguments show that no closed orbit can lie entirely above or below the $y = 0$ axis.) We begin with (\hat{y}_+, \hat{z}_+) solutions since the other possibility can be excluded. From (2.8), the asymptotic form of the $(0, 1)$ -solution is

$$\hat{y}_+ \sim \frac{1}{m} + \gamma \sin \omega t + \chi \cos \omega t, \quad \hat{z}_+ \sim \gamma \omega \cos \omega t - \chi \omega \sin \omega t, \quad (3.1)$$

with (possible) initial data given by $(t_o, y_o, z_o) = (0, 1/m + \chi, \gamma\omega)$. Thus the locus of points in phase space is in terms of the physical parameters (2.6)

$$\left(y_+ - \frac{W}{m}\right)^2 + \left(\frac{z_+}{\omega}\right)^2 = \frac{B^2}{(m - \omega^2)^2 + (2\omega\delta)^2} \equiv R^2. \quad (3.2)$$

This describes an ellipse centred on $(W/m, 0)$ with horizontal displacement R and vertical displacement ωR . Thus a *preloaded* (and physically benign) orbit may exist provided that the physical parameters satisfy

$$B < \frac{W}{m} \sqrt{(m - \omega^2)^2 + (2\omega\delta)^2} \equiv B_c. \quad (3.3)$$

We phrase the existence criterion in this way since in the numerical results section (§ 6), we concentrate on B and ω variation as these are the easiest to investigate experimentally. To illustrate (3.3) we set $W = 1$, $k = 10$ and $\delta = 0.01$, and plot Figure 1. Variation of W shows that this is a typical cross section. If B is fixed then there are three regimes. If B is very small

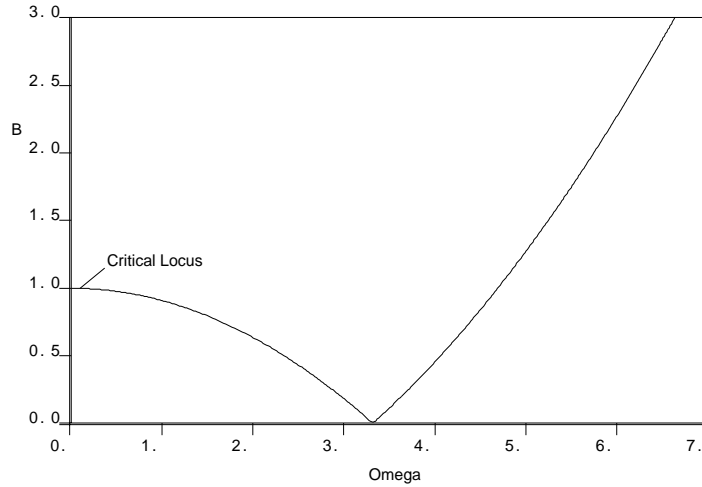


Figure 1: Existence windows for preloaded orbits (δ, W, k fixed; locus of B_c is shown).

(less than the minimum $2\delta W m^{-1/2}$ occurring at *linear* resonance), then the preloaded orbits exists for all ω . If $B > W$, then the preloaded orbits only exists for sufficiently large ω (the threshold is asymptotically $B \sim W\omega^2/m$). This is the case where the righthand side of (2.5) becomes two-signed. In between, there are two existence windows for preloaded orbits, and it is in this regime that one of the main continuations in § 6 takes place. Conversely, if ω is fixed, there is always a lower existence window in B . Note that taking $m = 1$ in equation (3.2) shows that no asymptotic response can lie entirely the lefthand side of the phase plane.

Before considering more complicated periodic responses, we note that the stability of the preloaded orbits can be analysed by using the stroboscopic map \mathcal{S} , where $\mathcal{S} : (y_o, z_o) \rightarrow (y_+, z_+) \equiv (f(y_o, z_o), g(y_o, z_o))$. Evaluating at $t = t_o + \frac{2\pi}{\omega}$, we obtain the eigenvalues as $\lambda_{\pm} = e^{-2\pi\delta/\omega}(c_{\omega} \pm s_{\omega})$ where c_{ω} and s_{ω} are the evaluated circular functions. While it exists, the preloaded orbit will be locally stable as a fixed point of the strobe map and hence as a periodic orbit of the differential equation. We plot typical preloaded orbits and study their interaction and coexistence with other kinds of orbits in § 6.

4 Existence of $(1, n)$ -Periodic Orbits

We now describe a largely analytical procedure for constructing $(1, n)$ asymptotic periodic responses. In the next section, we show how the same calculation can be used to determine their stability and bifurcation points. We consider that the response has settled down to a steady motion. Suppose that at a time t_o , the trajectory passes through the P -Poincaré plane at velocity z_o (and thus $y_o = 0$). Let t_1, z_1 denote the phase and velocity when it passes through $y = 0$ but with $z < 0$, and let t_2, z_2 denote the phase and velocity when it returns to the P -plane and the periodic motion is completed. We refer to Figure 2. The following conditions will then hold

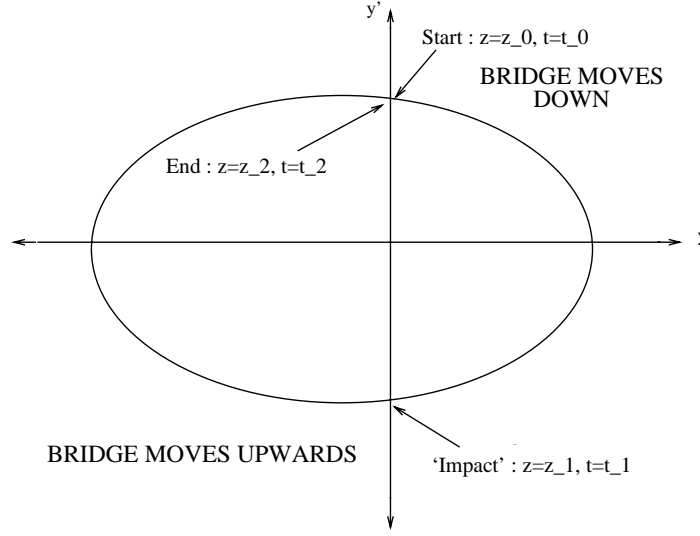


Figure 2: Notation for a $(1, n)$ -asymptotic periodic response.

$$t_2 = t_o + \frac{2n\pi}{\omega}, \quad (4.1)$$

$$\hat{y}_+(t_1) = 0, \quad (4.2)$$

$$\hat{z}_+(t_1) = \hat{z}_-(t_1), \quad (4.3)$$

$$\hat{y}_-(t_2) = 0, \quad (4.4)$$

$$\hat{z}_-(t_2) = \hat{z}_+(t_o). \quad (4.5)$$

Thus we have 5 equations in 5 unknowns and, as might be hoped, we can indeed solve for them all. Following (Hogan 1989), this is done by first solving for the time difference $\Delta t = t_1 - t_o$. Since the relationships (4.1-4.5) define the quantities implicitly, they have to be manipulated until (eventually) one obtains a nonlinear, transcendental equation for Δt . This is then solved numerically. All other orbit parameters can then be found via substitutions. Note that t_2 can be replaced wherever it appears right from the outset via use of (4.1). Although the calculations are lengthy, the results do provide an independent check on any numerical solutions. Moreover, the more complicated solutions often have very small basins of attractions, especially near bifurcations. It is extremely unlikely that suitable initial data for the numerical solver would be found by chance. Our approach makes such orbits accessible and allows for some basic continuation of solutions. Note that the output from this procedure has to be scaled appropriately before comparison is made with numerical solutions of (2.5), because of the use of the extra scaling to simplify algebra.

We sketch the solution procedure and state the results, but omit all details for the sake of brevity. Equation (4.2) is rearranged to yield of the form

$$z_o = F(c_i, s_i, \Delta t) \quad (4.6)$$

where $i = 1, 2$ and F is also a function of the parameters (2.6). Similarly, using the fact that

$t_2 - t_1 = 2n\pi/\omega - \Delta t$, we obtain an equation

$$z_1 = G(c_i, s_i, \Delta t) \quad (4.7)$$

from (4.4). Next, with the help of (4.3,4.5), we obtain other expressions for z_o and z_1 so that they may be eliminated to obtain equations solely in the c_i and s_i . This yields a linear system which we write as

$$\mathcal{A}c_o + \mathcal{B}s_o = \mathcal{C}c_1 + \mathcal{D}s_1 + \Xi, \quad (4.8)$$

$$\mathcal{E}c_o + \mathcal{F}s_o = \mathcal{G}c_1 + \mathcal{H}s_1 + \Theta. \quad (4.9)$$

The coefficients are functions of the system parameters and Δt and are given in the Appendix. The dependence on t_1 is removed by writing $t_1 = \Delta t + t_o$ and expanding the circular functions. We then solve for c_o and s_o and use the fact that $c_o^2 + s_o^2 = 1$ to finally obtain the nonlinear equation for Δt ,

$$(\mathcal{D}'\Xi - \mathcal{B}'\Theta)^2 + (\mathcal{A}'\Theta - \mathcal{C}'\Xi)^2 - (\mathcal{A}'\mathcal{D}' - \mathcal{B}'\mathcal{C}')^2 = 0, \quad (4.10)$$

where the primed versions of coefficients are given in the Appendix. Equation (4.10) can be simplified a little further but there is little advantage in doing so. In practice, the equation was solved by bisection to 10 decimal places at each root within the relevant interval $(0, 2n\pi/\omega)$. A double root corresponds to a fold bifurcation point and thus does not raise problems. Once Δt is known, we can obtain t_o from

$$t_o = \frac{1}{\omega} \arctan \frac{\mathcal{A}'\Theta - \mathcal{C}'\Xi}{\mathcal{D}'\Xi - \mathcal{B}'\Theta}. \quad (4.11)$$

One can then calculate all the individual times via use of (4.1) and thence z_1 and z_o from the explicit solutions. Thus the solution can be plotted and initial data for a numerical solver generated.

However, not all the roots generated in the interval are physical. Some are spurious (generated by manipulations such as squaring or corresponding to ‘integrating’ with an equation in the wrong half of phase space) whilst others might be copies (up to phase). This means that the procedure requires some intervention to discard roots after plotting. When a period doubling bifurcation occurs, a simple root of (4.10) ceases to lie in the interval (for a given n). Locally, the bifurcation should be $(\ell, n) \rightarrow (2\ell, 2n)$ and hence we cannot with the above method calculate analytically the period $2n$ solution. Our approach could be extended to the case $\ell > 1$ but the analysis is even more complicated and is not pursued here. Globally, of course, the solution type is likely to change (see § 6). For a fold bifurcation, the two roots can be relevant: the second corresponding to an *unstable* solution. (We plot such a solution in § 6, which could not be found by simple numerical simulation.) However, away from the bifurcation, the second root can cease to be physical through a global event or simply because it passes outside the possible interval. In fact, if the minimum of (4.10) lies under the endpoint of the feasible interval then the unstable solution would never be admissible, even local to the bifurcation point.

5 Orbital Stability of $(1, n)$ Orbits

The asymptotic responses found by the (largely) analytical method described above need not be stable. The presence of any perturbation (to the actual initial data) can lead the system settling onto another (stable) orbit which may or may not be periodic. We carry out the stability analysis in the manner of (Hogan 1989). However, we present an easier way of deriving expressions for the determinant and trace of the pertinent Jacobian matrix. The analysis is carried out in the phase plane using the Poincaré map P : the periodic orbit is a fixed point of the map. We use the previous notation for labelling a given periodic response. The stability of fixed point (and thus the asymptotic response) is determined by the eigenvalues of the Jacobian DP (Guckenheimer & Holmes 1986).

The calculation of DP proceeds in two parts, depending upon which equation is being integrated. That is, we decompose the map $P = P_- \circ P_+$ where

$$P_+ : \begin{pmatrix} t_o \\ z_o \end{pmatrix} \mapsto \begin{pmatrix} t_1 \\ z_1 \end{pmatrix} = \begin{pmatrix} f(t_o, z_o) \\ g(t_o, z_o) \end{pmatrix}, \quad P_- : \begin{pmatrix} t_1 \\ z_1 \end{pmatrix} \mapsto \begin{pmatrix} t_2 \\ z_2 \end{pmatrix} = \begin{pmatrix} h(t_1, z_1) \\ \kappa(t_1, z_1) \end{pmatrix}. \quad (5.1)$$

We begin by studying P_+ whose Jacobian

$$DP_+ = \begin{pmatrix} \frac{\partial f}{\partial t_o} & \frac{\partial f}{\partial z_o} \\ \frac{\partial g}{\partial t_o} & \frac{\partial g}{\partial z_o} \end{pmatrix} \quad (5.2)$$

has entries which may be determined by the implicit differentiation of the defining equation (4.2) for t_1 (and then that of z_1). We use the Chain Rule to deduce that

$$\frac{\partial f}{\partial t_o} = - \frac{1}{\hat{z}_+(t)} \bigg|_{t=t_1} \left(\frac{\partial \hat{y}_+}{\partial t_o} \right) \bigg|_{t=t_1}, \quad \frac{\partial g}{\partial t_o} = \frac{\partial^2 \hat{y}_+}{\partial t^2} \bigg|_{t=t_1} \frac{\partial f}{\partial t_o} + \frac{\partial \hat{z}_+}{\partial t_o} \bigg|_{t=t_1}, \quad (5.3)$$

$$\frac{\partial f}{\partial z_o} = - \frac{1}{\hat{z}_+(t)} \bigg|_{t=t_1} \left(\frac{\partial \hat{y}_+}{\partial z_o} \right) \bigg|_{t=t_1}, \quad \frac{\partial g}{\partial z_o} = \frac{\partial^2 \hat{y}_+}{\partial t^2} \bigg|_{t=t_1} \frac{\partial f}{\partial z_o} + \frac{\partial \hat{z}_+}{\partial z_o} \bigg|_{t=t_1}. \quad (5.4)$$

When these equations are evaluated, the second derivative term in y_+ can be simplified using the differential equations (2.5). That is,

$$\frac{\partial^2 \hat{y}_+}{\partial t^2} \bigg|_{t=t_1} = -2\delta \hat{z}_+(t_1) - m\hat{y}_+(t_1) + 1 + F s_1. \quad (5.5)$$

One can evaluate the derivatives in the style of (Hogan 1989) and obtain the complicated expressions given in the Appendix. From such formulae, one can obtain the entries of DP_+ . However, if the focus is not on the specific expansion in a given direction, it is simplest to explicitly evaluate little of (5.3-5.4) and, using the fact that $\hat{y}_+(t_1) = 0$ to simplify (5.5), instead calculate the determinant and trace more directly. The eigenvalue stability problem for P is given by

$$\lambda^2 - (\text{trace } DP)\lambda + (\det DP_- \det DP_+) = 0, \quad (5.6)$$

where

$$\text{trace } DP = \frac{\partial h}{\partial t_1} \frac{\partial f}{\partial t_o} + \frac{\partial h}{\partial z_1} \frac{\partial g}{\partial t_o} + \frac{\partial \kappa}{\partial t_1} \frac{\partial f}{\partial z_o} + \frac{\partial \kappa}{\partial z_1} \frac{\partial g}{\partial z_o}. \quad (5.7)$$

Now for any simple trajectory through the phase plane,

$$\det DP_+ = e^{-2\delta\Delta t} \frac{z_o}{z_1} \quad (5.8)$$

and similarly for $\det DP_-$. Combining these results for a complete periodic asymptotic response and using 4.1, we obtain that

$$\det DP = e^{-4n\pi\delta/\omega} < 1. \quad (5.9)$$

Hence there can be no Hopf-Neimark bifurcations to quasiperiodic motions and one eigenvalue always remains inside the unit circle. Moreover, in general

$$\det DP = e^{-2\delta\Delta t} \frac{z_o}{z_2} \quad (5.10)$$

so that the determinant is unbounded at $z_2 = 0$. Therefore P is not differentiable in this case. (This is to be expected as the situation is analogous to that for ‘grazing bifurcations’ in impact oscillator theory). As no Hopf-Neimark bifurcations occur, the stability boundaries are $\lambda = \pm 1$. Using the method described above to calculate the trace, we find that a large number of terms cancel to yield for a periodic asymptotic response

$$\text{trace} = e^{-2n\pi\delta/\omega} \left(2c_m c_\delta - \frac{s_m s_\delta (m + 1 - 2\delta^2)}{\sqrt{(1 - \delta^2)(m - \delta^2)}} \right), \quad (5.11)$$

where, additionally,

$$c_\delta = \cos \sqrt{1 - \delta^2}(t_2 - t_1), \quad s_\delta = \sin \sqrt{1 - \delta^2}(t_2 - t_1). \quad (5.12)$$

The divergence or fold bifurcation occurs when $(\text{trace} - \det) = 1$ and the flip or period doubling bifurcation when $(\text{trace} + \det) = -1$. Both these quantities can be evaluated and monitored as we continue an analytical orbit ‘by hand’, using the method described previously to evaluate all parameters and solution constants. Thus different kinds of bifurcations can be found in readiness for checking with the numerical integrations. In fact, for much of the time that the orbit is stable, the eigenvalues form a complex conjugate pair on the circle whose squared radius is given by the value of $\det DP$. However, before either a fold or a flip occurs, the eigenvalues coalesce on \mathbf{R} . The eigenvalues then move in opposite directions, so that after the bifurcation, one lies inside the unit circle and one outside. However, the piecewise linear nature of the system has repercussions for the prediction of the number of solutions. We have mentioned this already for folds: if one has a stable solution close to a fold, the unstable solution may not exist. Moreover, one would expect the ‘period-one’ solution to persist at a flip but this may not be the case.

6 Numerical Results

In this section, we trace out a number of paths in parameter space. In doing so, we try to illustrate the rich dynamic behaviour possible: the coexistence of sub and superharmonic solutions, period-doubling and -adding sequences, truncated cascades, fold bifurcations and global

bifurcations. We concentrate on a variation of B with all parameters fixed, and similarly, one of ω . We also exhibit a period-doubling cascade with k . The choice of parameters has been somewhat arbitrary. When the beam experiments are undertaken, actual values for the physical parameters can be properly estimated. Meanwhile, the analytical relationship between a full bridge model and the beam model is unclear. At present, it seems productive and useful to first understand the full range of dynamics in this simple model. The transitions between solution types and patterns of coexistence are certainly more complicated than one might naïvely think.

As mentioned in the introduction, parameter values given in this section correspond to the natural scaling (2.6) of the ODEs in order to allow physical interpretation of all the diagrams in terms of the type of suspension bridge we are modelling. We do not wish to unnecessarily constrain the dynamic behaviour, and hence keep damping fairly small (usually $\delta = 0.01$) and the asymmetry in the system moderately large (typically $k = 10$). We also wish to take proper account of the preload W : it seems that it is when $B \gg W$ that the complete cascades are possible. It may be possible to investigate this analytically in the manner of Elvey and Thompson (Elvey 1983). The slight parameter redundancy in our nondimensionalisation allows us to identify in a transparent way when physically small forcing terms are associated with orbits whose magnitude is much larger. However, this phenomenon occurs *away* from linear resonance values. Indeed, at such values, behaviour is often relatively benign.

In the next two sections, we compare analytical results with those obtained by direct simulation of equations (2.5) (using NAG routine `d02cjf`) and by parameter continuation using the package AUTO (Doedel & Kernevez 1986). The AUTO code continues the periodic orbits as fixed points of the P^m -Poincaré map (with the relevant power) upon the z -axis intercept. The intermediate swaps between (y_+, z_+) and (y_-, z_-) solutions are obtained internally by Newton iteration, and passed as parameters to allow restarting of continuation. When the code reaches an end point of an (ℓ, n) orbit, examination of the AUTO output usually allows the identification of changes in ℓ via the extinction of a loop, or its passing into the righthand plane. The semi-analytical method is used to generate the highly accurate initial periodic orbits and swap times required to successfully begin continuation (especially of higher order orbits). The nonlinear equation (4.10) for $t_1 - t_o$ is itself unsuitable directly for exhaustive automated continuation. (For that reason, Figures 8 & 9, for example, were produced using AUTO.)

6.1 Variation of ω

For these variations, we set $W = 1$ and $B = 0.5$. The bifurcations in this direction all seem to be folds. A given full phase space (ℓ, n) -orbit exists in a *window* of ω values, and disappears through a fold at each end. However, the orbit geometry is not symmetric with respect to this window. In line with the findings of (Lazer & McKenna 1991) for the floating beam model of a ship, it is at the lower ω end that the large scale oscillations may be found. For (Lazer & McKenna 1991), this finding is important since the floating beam is a common model in naval architecture, and the indicated relationship clashes with a common safety procedure. These large scale oscillations persist over a significant parameter sub-window. With reference to the

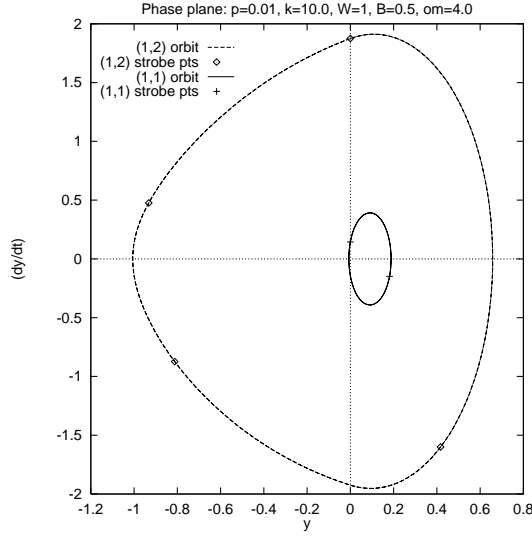


Figure 3: Subharmonic coexistence of $(1,1)$ and $(1,2)$ -orbits ($\delta = 0.01$, $k = 10$, $\omega = 4$, $W = 1$, $B = 0.5$).

suspension bridge model, we emphasize that *they are not the result of narrow linear resonance*.

We begin with a $(1,2)$ -orbit at $\omega = 4$. Via the analysis of § 4, we find that possible initial data for this orbit is the \mathcal{S} -Poincaré point $(t, y, z) = (0.60977664, -0.81204135, -0.87377383)$ (of course, P -map initial data with $y = 0$ cannot be directly used). In addition, § 5 assures us that this orbit is stable. Direct numerical integration confirms these figures in full. For the sake of brevity, we abbreviate numerical values in the sequel. The simplest, effective way to move around parameter space with the numerical solver (as opposed to AUTO) is to use the Poincaré point as the starting conditions for a slightly different value of ω , and then integrate until a new asymptotically stable trajectory is found. At the same point in parameter space, we can also find a $(1,1)$ orbit of which the $(1,2)$ -solution is a subharmonic. Both are shown in Figure 3. In this and all subsequent phaseplanes, strobe points corresponding to intervals of π/ω (rather than $2\pi/\omega$) are shown. This is in order that for low n (m, n) orbits, the speed of tracing out each part of the orbit is more evident.

The $(1,1)$ -orbit is (at this moment) a small amplitude orbit whereas the $(1,2)$ -orbit is a large scale motion with an amplitude 4 times the magnitude of the forcing term. If we continue the $(1,2)$ orbit, we find that it undergoes fold bifurcations at $\omega = 3.28$ and $\omega = 6.56$. Local to these bifurcations, we thus have at least three solutions coexisting; the third being an unstable $(1,2)$ orbit. Note that the stable eigenvalues sit on a circle of changing radius as they tend to \mathbf{R}^+ prior to passing through $+1$, according to (5.9). Throughout this window, the $n = 1$ orbit persists but it passes entirely into the right hand plane (to become a $(0,1)$ -solution when $\omega \sim 4.06$, see § 3). Figure 4 illustrate the relative sizes of the two kinds of orbits at either end of the $n = 2$ existence window.

The calculations of § 3 show that the preloaded orbit exists for all larger ω . What happens if

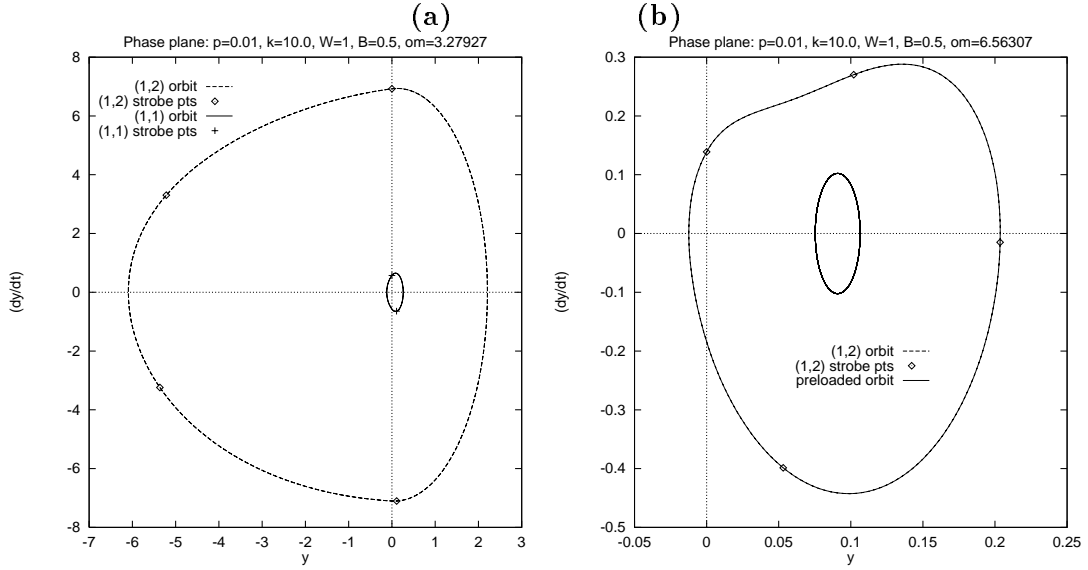


Figure 4: Comparison of coexisting subharmonics near to fold points. (a) $\omega = 3.27927$, (b) $\omega = 6.56307$.

the (1,1)-orbit is continued by decreasing ω ? The theory indicates that it disappears through a fold bifurcation when $\omega \sim 1.57$. In this case, the expansion is even more dramatic: the y displacement is highly asymmetric, and the amplitude is up to 50 times the magnitude of the forcing (see Figure 5). This (1,1)-orbit coexists with a small preloaded (0,1)-orbit which appears (§ 3) when $\omega \sim 2.35$.

Apart from any other (unstable) solutions, the symmetric (1,1)-orbit can also coexist with a *superharmonic* asymmetric (1,1)-orbit which is close in size to the preloaded orbit. This ‘extra’ (1,1)-orbit appears when $\omega \sim 1.65$ and has a loop in the righthand side of phase space. (In Figure 6 (a), we show only the nonstandard (1,1)-orbit with the preloaded orbit; the usual (1,1) involves displacements up to 8 in magnitude.) As the superharmonic is continued by decreasing ω further, it undergoes a ‘period-adding bifurcation sequence (in ℓ). That is, the inner loop crosses $y = 0$ to form a (2,1) orbit when $\omega \sim 1.64$, a different type of subharmonic coexistence for the ‘standard’ (1,1)-orbit than previously (see Figure 5 (b)).

Using the method of § 4, it is straightforward to find higher order subharmonics. As expected, these are to be found in existence windows at higher values of ω . For example, there is a (1,3)-orbit which exists between fold bifurcations at $\omega \sim 5.38$ and $\omega \sim 7.25$. This hence initially coexists with the preloaded and (1,2)-orbits with which we began this section. The *variation* of amplitude is as before, but again, by increasing n , the maximum amplitude is reduced (see Figure 7).

The next set of figures were obtained using AUTO and give a more global view of the transitions, as well as uncovering new phenomena. In Figure 8, all the first three regular harmonics are shown, and the increase in size with *decreasing* frequency is dramatic. (Dashed lines indicate unstable orbits.) Note that the z -axis intercept is *not* the maximum z displacement. Observe,

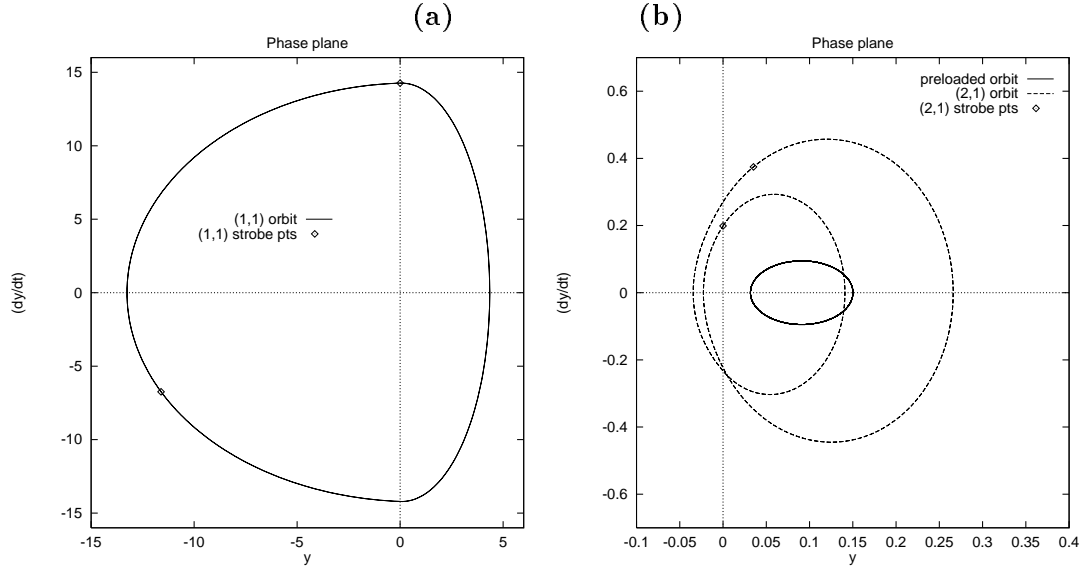


Figure 5: Multiple coexistence close to the (1,1)-orbit fold bifurcation point ($\omega = 1.6$).

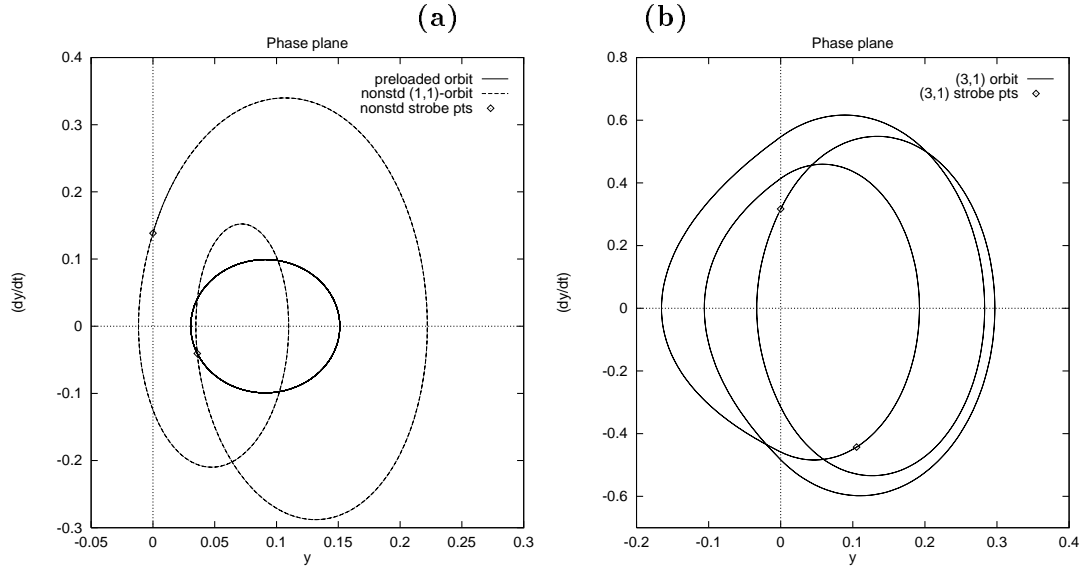


Figure 6: (a) Superharmonic coexistence of full orbits: Nonstandard (1,1)-orbit at $\omega = 1.645$
(b) (3,1) orbit arising through period adding ($\omega = 0.95$).

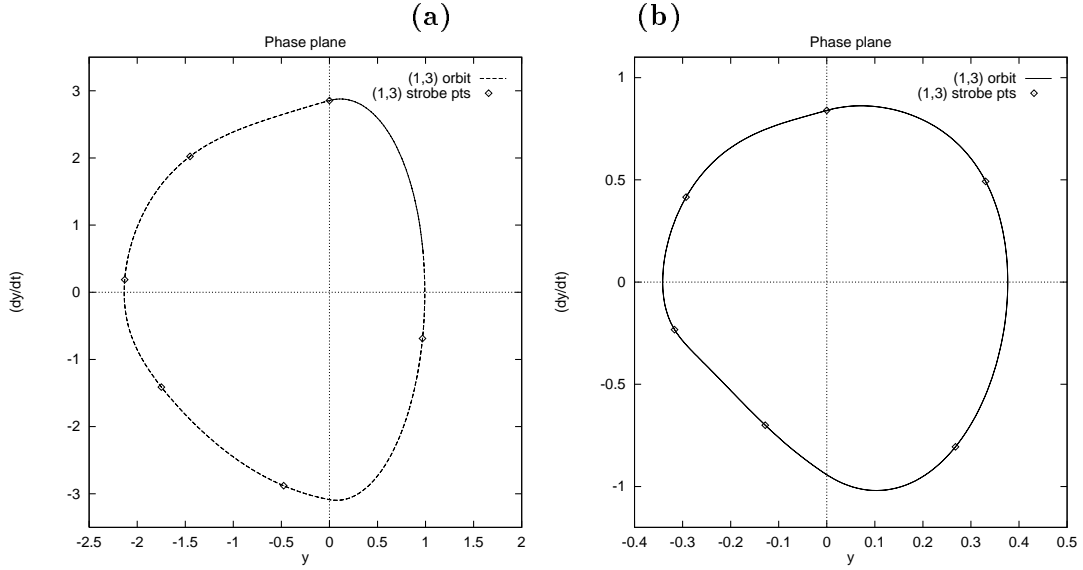


Figure 7: Higher subharmonics – a (1,3)-orbit (a) near lower fold $\omega = 5.38495$ (b) near upper fold $\omega = 7.252321$.

too, that for any (ℓ, n) orbit we only plot one point per orbit to simplify the diagram. This point corresponds to a particular crossing which is representative of its amplitude. In Figure 9, we focus in on the appearance of the primary (1,1) harmonic from the preloaded orbit (PL), with the asymmetric orbits appearing to the left at lower values of ω . Of course, the preloaded orbit appears as the $z = 0$ axis since there is no intercept. Note, too, that the use of AUTO has revealed the additional coexistence of two *stable, symmetric* (1,1) orbits between the PL point and the first change of stability at a limit point (LP). This had not been observed by much direct numerical simulation, but had been suspected since we know the preloaded orbit to be stable.

In Figure 10, we focus on the asymmetric orbits. (The isola is labelled in a clockwise fashion.) For the second of these, the ‘period-adding’ is extended to include a (3, 1) orbit (shown in Figure 6 (b)). Moreover, the isolas in these figures do not *physically* cross. They maybe unfolded by plotting the parameter variation against both the z axis intercept and the phase of the solution. In Figure 11, this is shown for the regular third harmonic.

6.2 Variation of B

With the variation of B , one often encounters, in addition to folds, *period doubling* bifurcations. (In this section, and the next, note that the eigenvalues which predict bifurcation lie on a *fixed circle* prior to coalescence.) To illustrate this, we start with a ‘transverse’ variation to the standard (1,1)-orbit path treated above. We denote this as the primary branch in what follows. We begin with $\omega = 3$ and $B = 0.5$. First, we increase B (Figure 12). The first period-doubling bifurcation occurs at $B \sim 2.83$, that is, $(1,1) \rightarrow (2,2)$. Before then the orbit has coexisted

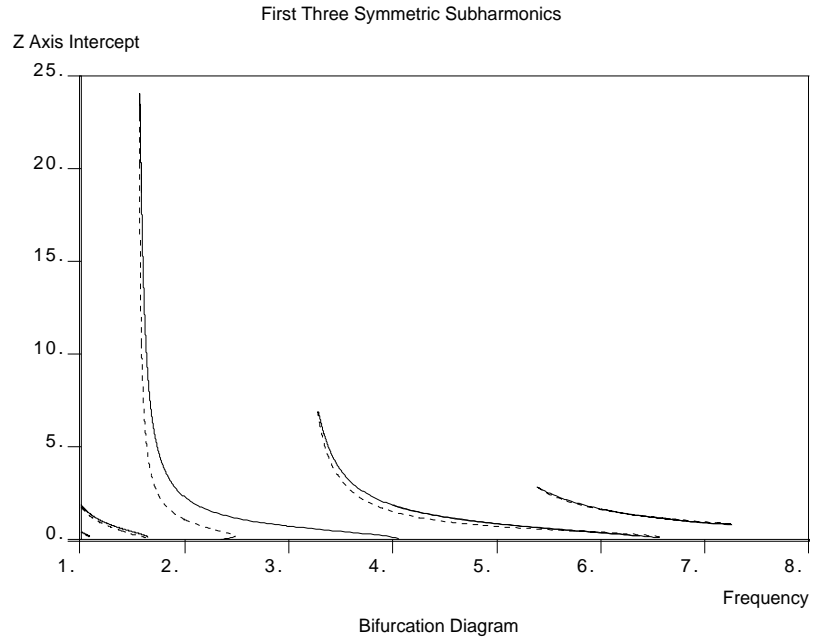


Figure 8: Amplitude magnification for decreasing frequency. (First three subharmonics.)

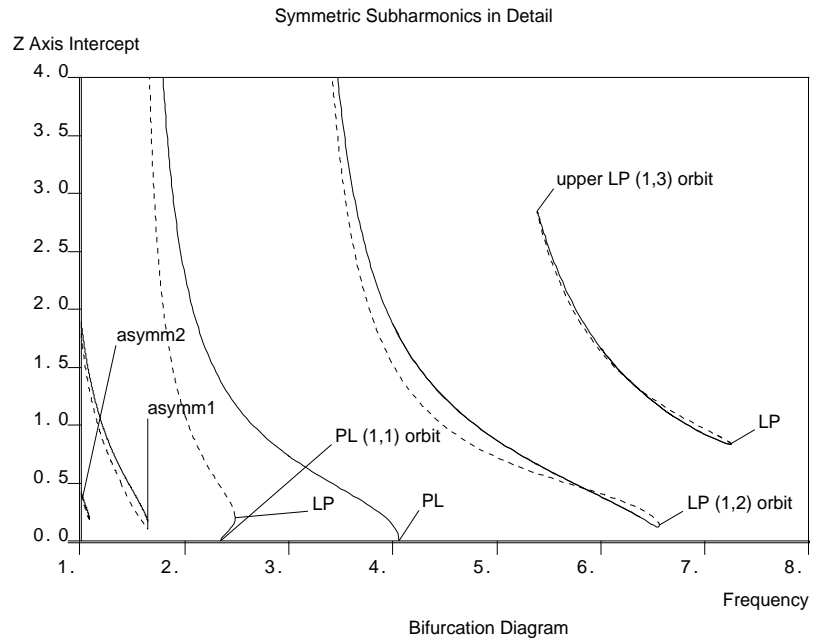


Figure 9: Focus on birth of the (1, 1) orbit from the preloaded state.

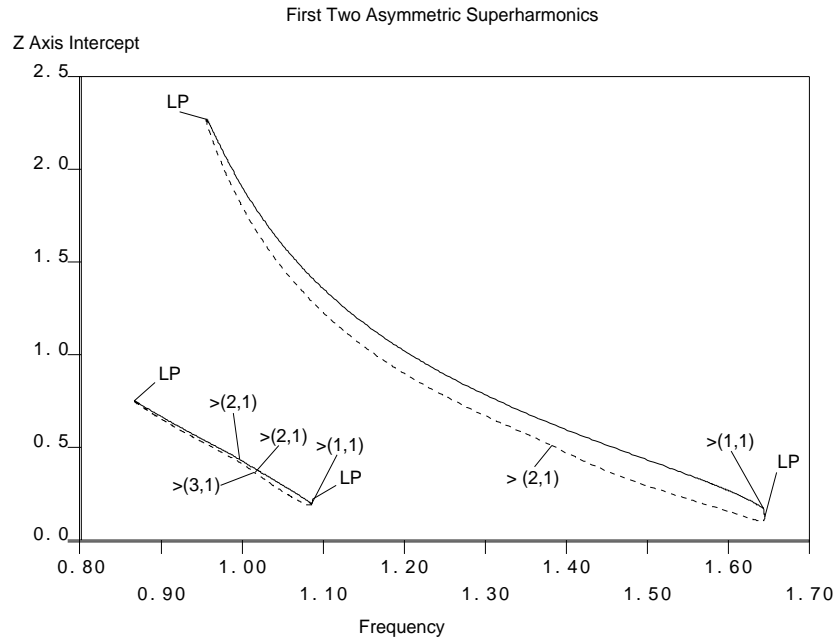


Figure 10: Asymmetric orbits, with ‘period-adding’ in ℓ .

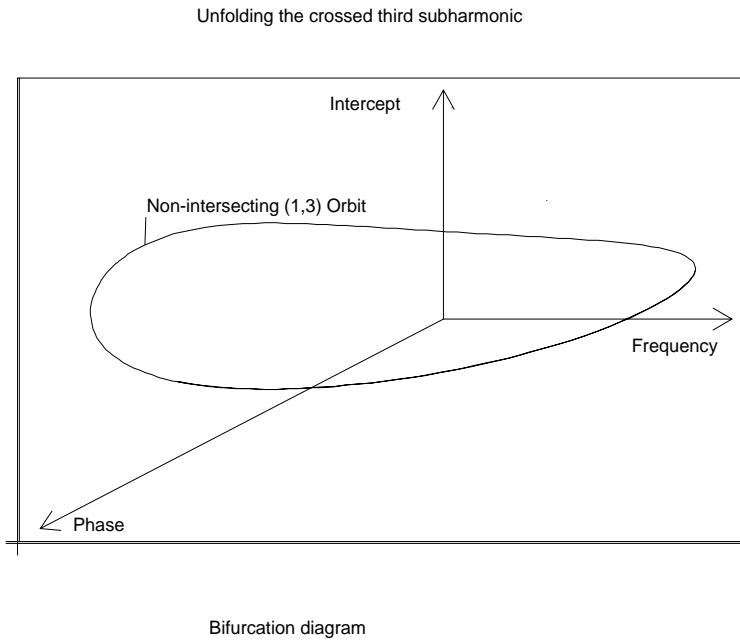


Figure 11: A crossed isola is unfolded by introducing the phase into the bifurcation diagram.

with, for example, a $(3,3)$ -orbit (Figure 17 (a)). Locally, the period-doubling bifurcation is $(1,1) \rightarrow (2,2)$ but the inner loop shrinks as B increases further and the outer loop stretches increasingly asymmetrically into the lefthand plane. When $B \sim 4.63$ the inner loop hits the origin and undergoes another period doubling bifurcation to an (incipient) $(4,4)$ -orbit. However, as the inner loop bifurcates, one new loop moves into the left hand plane and the other, entirely into the righthand plane. Hence instead a $(2,2) \rightarrow (3,4)$ bifurcation is actually observed. This is an instance where a bifurcation is complicated by the piecewise linear nature of the system. However, unlike the fold bifurcations, the orbits (though nonlinear) do not have large-scale amplitudes relative to the *forcing*.

In smooth bifurcation theory, one would now expect a cascade of such bifurcations. In impact oscillator models, they are often interrupted by grazing bifurcations. In our case, two things happen. First, once $B \sim 6.2$, a loop has passed through $y = 0$ and a $(3,4) \rightarrow (2,4)$ transition has taken place. Then the period doubling cascade is truncated by the ‘reverse’ bifurcation to a $(1,2)$ -orbit when $B \sim 6.491$. This bifurcation point can be analytically determined. As B is increased further, this orbit undergoes no other bifurcation. When $B \sim 11.6$, the extra loop in the right hand plane disappears and a curve enclosing a convex region remains.

In Figure 13, we show the same transition as produced by the AUTO code. Note the sharp increase in the z axis intercept which is associated with the gain of orbit convexity (and symmetry) in phasespace of the $(1,2)$ orbit. The period doubling is shown in more detail in Figure 14, where the transitions of the unstable orbit are also indicated. The total effect of the transition is turn a first into a second harmonic. In addition, the proximity of the LPs on the $(3,4)$ branch to the PD point indicate that nearby in parameter space is a (codimension two) generalised flip or Bautin bifurcation.

If we decrease B from the start value of 0.5, the behaviour is rather different. The $(1,1)$ -orbit disappears through a fold bifurcation at $B \sim 0.0097$. Note that once $B < 0.18$, a preloaded orbit also exists. In Figure 15, we show the stable and unstable solutions which exist near the fold point (the difference $(\text{Tr} - \text{Det})$ is 0.9), as well as the preloaded solution. In Figure 16, we show the hysteresis curve as produced by AUTO. As for the ω variation, there is restabilisation of the $(1,1)$ orbit through a fold in line with the calculations of § 2. It was this feature that was subjected to extended parameter variation of the full PDE in (Choi et al. 1991).

However, coexisting with the primary branch are a number of more exotic trajectories. As just two examples, for $B = 2.2$, we show in Figure 17(a) a $(3,3)$ -orbit and when $B = 8$, a $(4,6)$ -orbit (Figure 17 (b)). One would expect to find such higher order orbits for $B \gg W$. However, what becomes clear, with the use of a continuation code like AUTO, is that they persist at least to the regime where $B \sim W$, that they are interlaced with the primary branch and that they appear to be involved in the global bifurcation structure of the primary branch. For example, in Figures 18, 19, we show a high order transition and its relationship to the primary branch. The labelling is clockwise in Figure 18. Again, we are close to a codimension two bifurcation point. In Figure 20, we show an almost symmetric pair of solution branches of $(2,3)$ (and $(3,3)$) solutions. The loss of symmetry is probably due to the use of the z axis intercept as

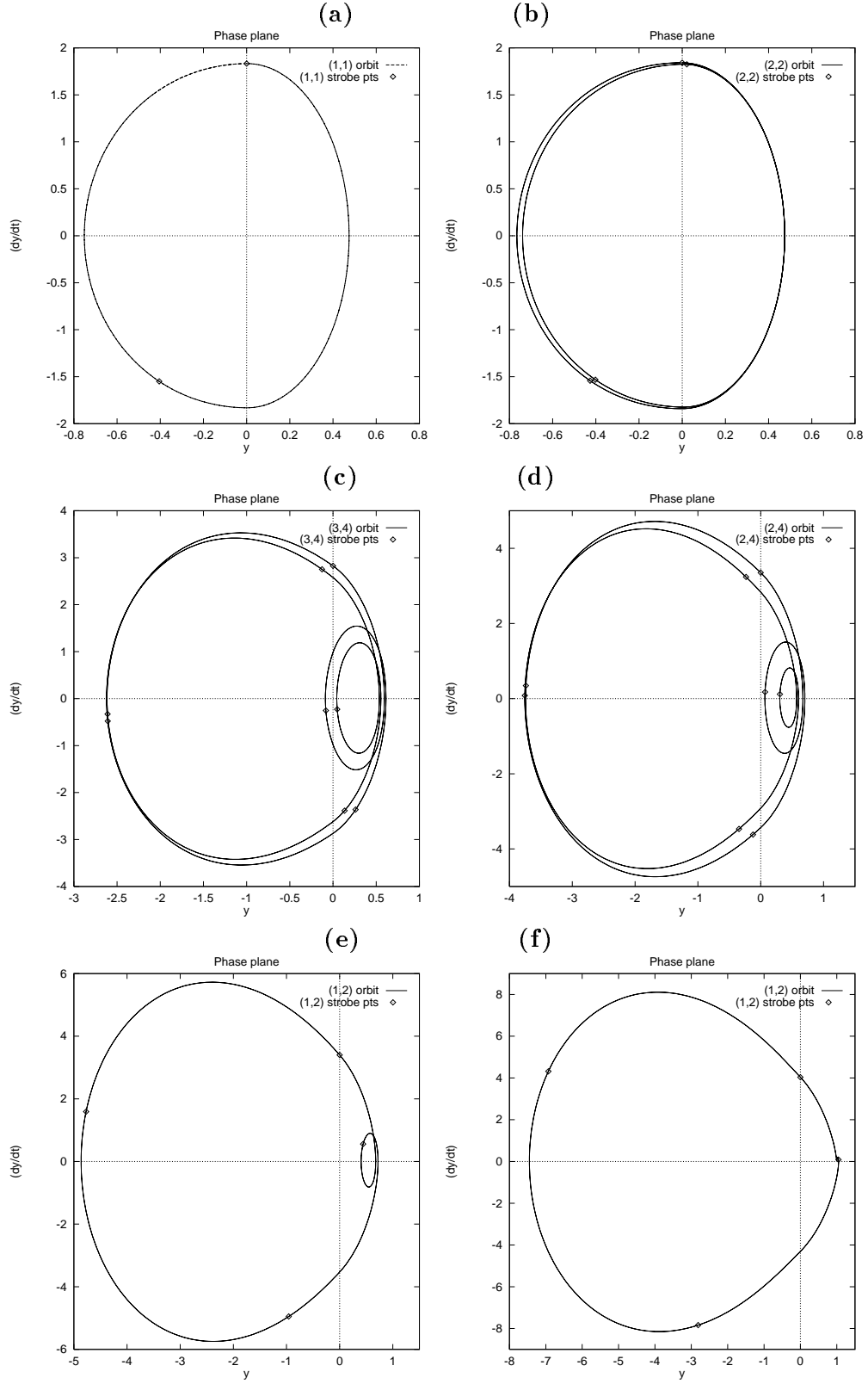


Figure 12: Truncated period doubling cascade in B (a) $B = 2.83$, (b) $B = 2.833$, (c) $B = 4.7$, (d) $B = 6.4$, (e) $B = 8.0$ and (f) $B = 10.8$.

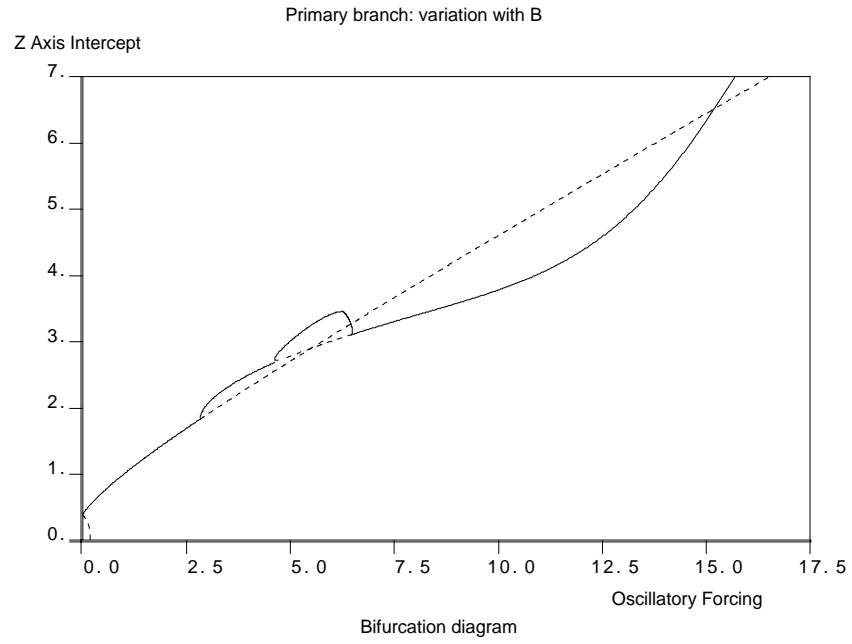


Figure 13: Global behaviour of the primary branch: see Figures 14 and 16 for local detail.

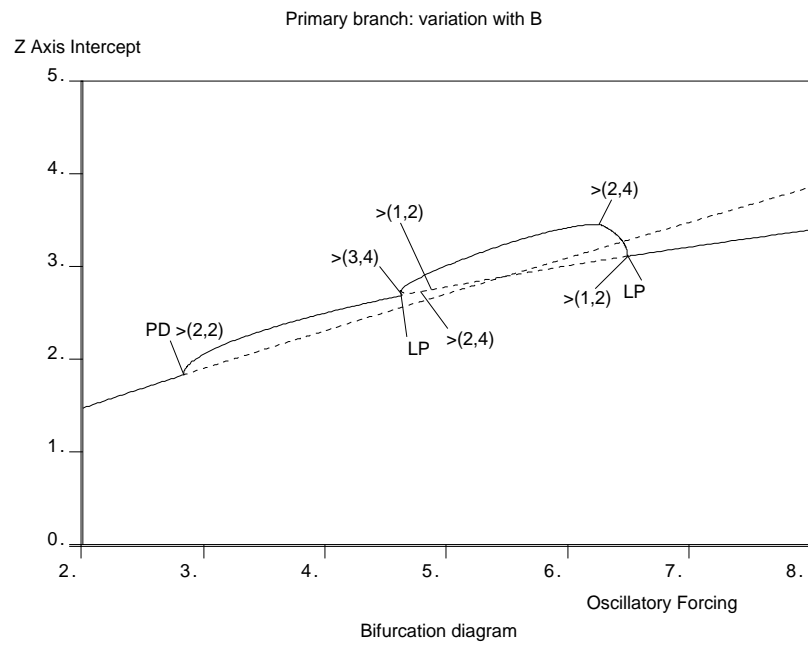


Figure 14: Truncated period doubling cascade.

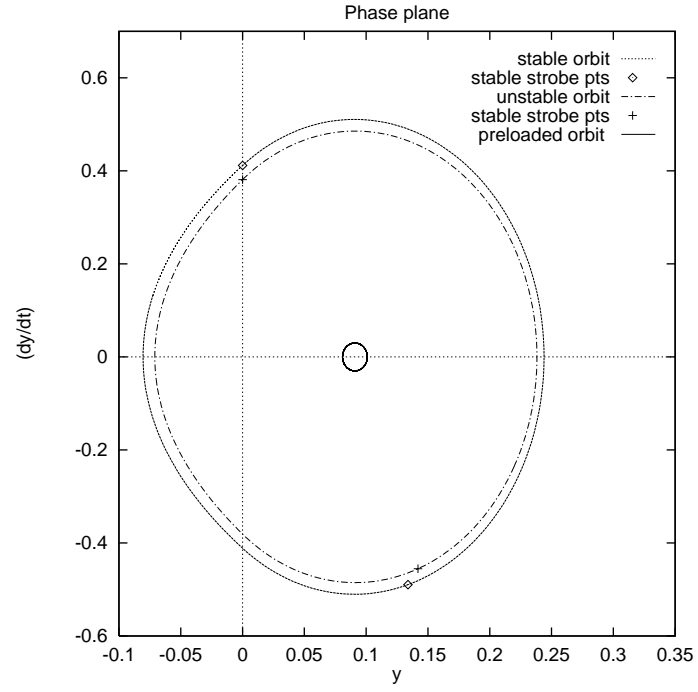


Figure 15: Stable (1,1), unstable (1,1) and preloaded (0,1) orbits when $B = 0.02$.

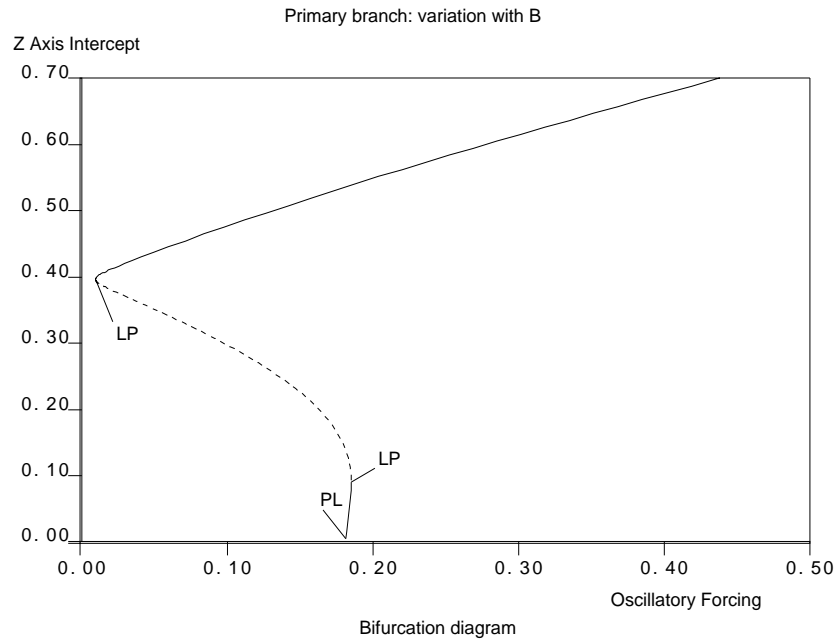


Figure 16: Hysteresis curve and transition of (1,1) orbit to the preloaded (0,1) state.

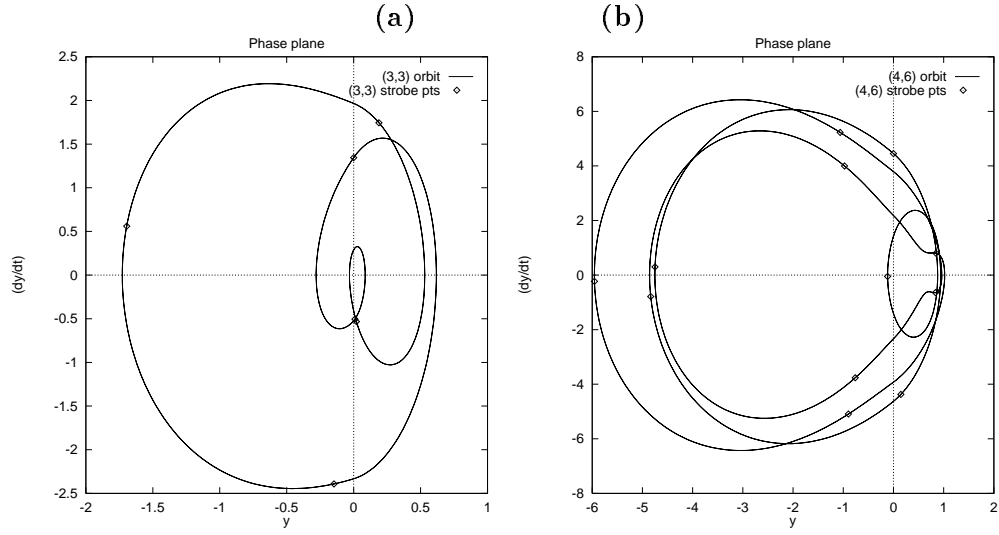


Figure 17: Complicated orbits coexisting with B variation primary branch. (a) (3,3)-orbit at $B = 2.2$, (b) (4,6)-orbit at $B = 8.0$.

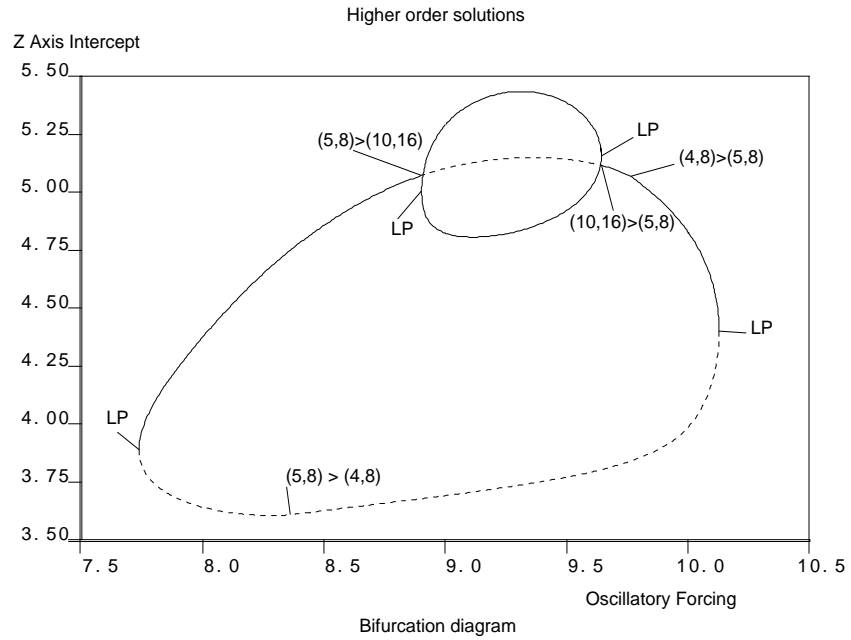


Figure 18: High order period doubling transition.

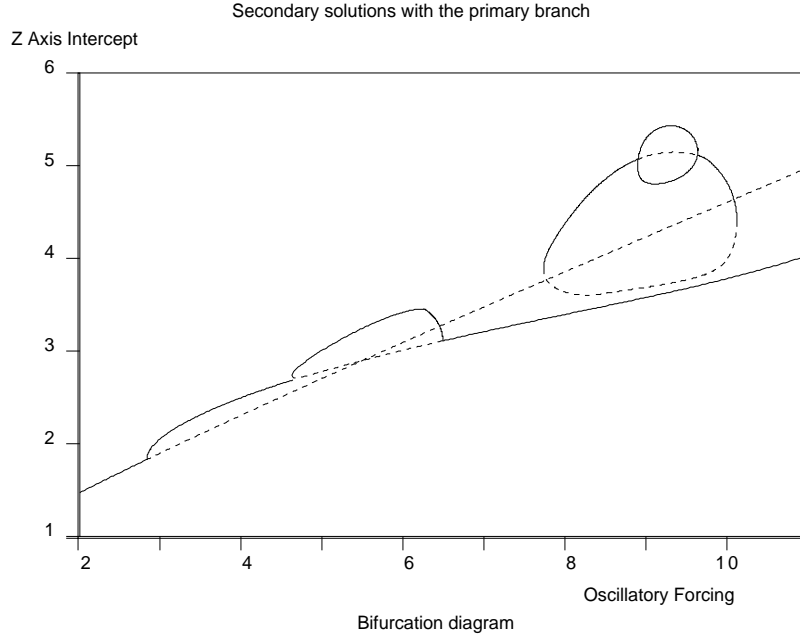


Figure 19: Relation of high order isola in Figure 18 to primary branch.

a measure of size in the bifurcation diagram, rather than a sup or L_2 norm, say. Note the coexistence of two *stable* (2,3) orbits from *different* solution branches. However, we were unable to extend the branches beyond the indicated end points (EP), which indicate some change in the solution type (ℓ, n) . There was some evidence of a limit point very close to the (3,3) EP, and similar structure on the other branches may have prevented AUTO from continuing period doubled branches, for example. (AUTO cannot, on its own, detect and follow codimension two bifurcations.) In Figure 21, we show coexistence of more exotic solutions, whose paths with respect to the bifurcation parameter are themselves highly complicated. Again, we show the primary branch for comparison.

6.3 Variation of k

Once $B \gg W$, the variation of k can yield (more) complete period doubling cascades relatively easily, even with greater damping in the system. Perhaps, it is unsurprising that, with strong forcing and increasing asymmetry in the system, exotic orbits can be obtained. We take $\delta = 0.05$, $\omega = 1$, $W = 0.1$ $B = 1$ and increase k upwards from $k = 1$. The initial data for the first orbit was found using the analytical methods: the first period doubling bifurcation occurs when $k \sim 6.3$ (analytically confirmed). As k is increased further, we obtain a sequence of periodic orbits with increasing close bifurcation k -values of which we have observed

$$(1, 1) \rightarrow (2, 2) \rightarrow (3, 2) \rightarrow (6, 4) \rightarrow (12, 8) \rightarrow (24, 16) \rightarrow \dots \quad (6.1)$$

This transition is featured in Figure 22: note how the period doubling appears associated with the intersection of loops with the $z = 0$ axis. Observe, too, the nonlinear dependence of the

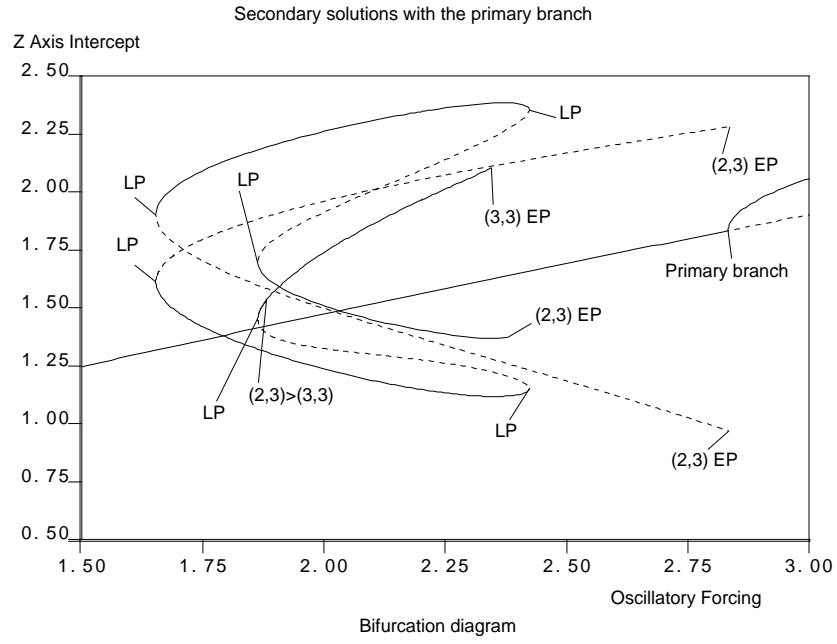


Figure 20: Almost symmetric pair of (2,3)-orbit pairs.

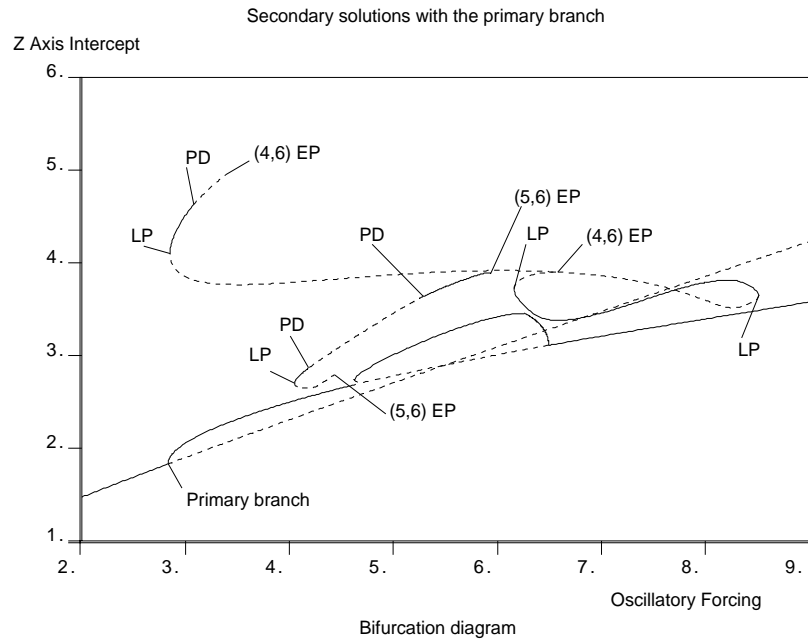


Figure 21: (4,6) and (5,6) orbits with the first subharmonic.

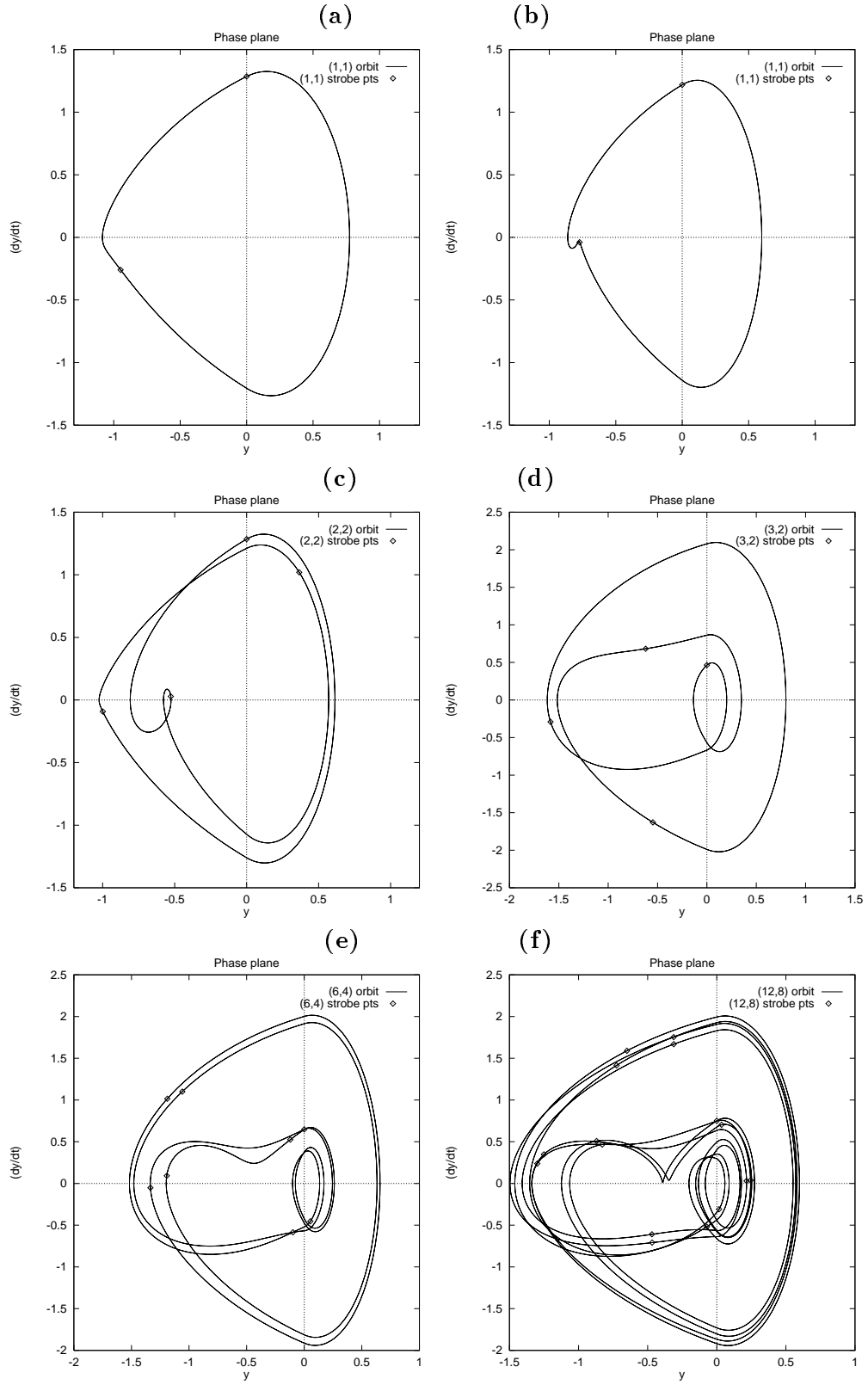


Figure 22: Period doubling cascade in k (a) $k = 4$, (b) $k = 6.2$, (c) $k = 6.5$, (d) $k = 8.0$, (e) $k = 11.0$ and (f) $k = 13.2$.

amplitude on the forcing for the bifurcating orbits. As for the truncated period doubling, that the ℓ entry of the orbit classification is more volatile than the ‘subharmonic’ label n . Yet the ℓ label remains important to distinguish full phase from ‘benign’ preloaded orbits. However, this parameter variation would be very difficult to investigate within an experimental framework, and hence we do not pursue it further here.

7 Conclusions

As a first step to understand the role of the ‘one-sided’ stay in suspension bridge dynamics, a suspended beam model has been considered. This represents the most complete analysis of the Lazer & McKenna model to date. We have revealed for the first time a great deal of nonlinear dynamics which will provide valuable input to experiments and higher dimensional models. Separation of variables was used to reduce the model to a piecewise linear ODE; which is equivalent to a one-sided preloaded forced spring, a case not studied before nor reducible to one that has. Methods have been given which enables two types of asymptotic periodic responses to be calculated. The second approach can yield unstable solutions which are otherwise inaccessible via direct numerical solution. A range of illustrative examples were then given which showed how the analytical methods may be used to structure a search of parameter space by simulation and continuation, and also the wide range of bifurcation phenomena and coexistence which are possible. Experimental verification of the results using a simple mechanical model is planned, and we hope to be able to report on this in the future. The choice of parameter variations was made with the problem of practical implementation in mind.

There is clearly plenty of scope for further analysis of this simple model. The basins of attraction of competing multiple solutions at a given point in parameter space have only been described anecdotally, rather than mapped. One would also like a more global structure for the coexistence possibilities. We have described one possible application of the continuation package AUTO (Doedel & Kerneves 1986). But much remains open. For example, are there infinitely many isolas of either regular $(1, n)$ subharmonics, and $(m, 1)$ asymmetric superharmonics; or is the number constrained like in the work of (Elvey 1983). And in the variation of B , the EPs of the $(2, 3)$ branches appear to coincide with the first period doubling of the primary branch: are some global dynamics responsible for this coincidence.

Recently, Fonda and co-workers (Fonda & Ramos 1991, Fonda, Schneider & Zanolin 1992) have used a different modification of the Lazer-McKenna model. They postulate a minimum height before slackening of the hangers, and (Brownjohn 1994) gives some support to this idea. They then choose to reduce the number of parameters by imposing a static balance effectively equivalent to a weightless bridge. (In addition, their analysis is largely concerned with the zero dissipation case.) In future work, the cutoff height could be incorporated into the analysis described here by modifying the separation of variables (2.3) with Heaviside functions. It is also important to note that part of their analysis assumed some symmetry in the shape and positioning of the orbits. None of the orbits we computed had any such symmetries. Other

authors (Choi & Jung 1991, Choi, Jung & McKenna 1993, Choi et al. 1991) have extended the work of Lazer & McKenna. For example, rotatory inertia has been incorporated into some of the theoretical results. We could do likewise, but the effect upon results is likely to be small.

Brownjohn (Brownjohn 1994) has also argued that, for two numerical case studies, the stay stiffness asymmetry is unimportant in the one dimensional motion. Of course, one might say that these are just two examples and that in postulating interactions for the finite element model, one may be imposing undue constraints. More importantly, it says nothing about the role of the asymmetry in determining stability and transitions. A number of modern long span suspension bridges have used mono-duo cables with *A*-frame tower construction (Ostenfeld & Larsen 1992). This reduces the importance of torsional dynamics in which the influence of the stays is most obvious. Nevertheless, from a theoretical perspective, it remains important to determine design and safety boundaries to prevent over and (under) design in future.

There remains a gulf between the ODE model we have studied and the beam equation, and an even larger one between that and a complete bridge model. However, it is to be hoped that demonstrating the dynamic complexity of the simplest model is a useful task with some relevance to more complicated ones. The priority is the inclusion of torsion via some route, whether through PDE analysis or the coupling of ODE models. Whichever proves most fruitful, it seems clear that the positive use of the piecewise linear nature of the system, along with nonlinear dynamics, can provide new and useful information compared to the nonlinear analysis employed by Lazer, McKenna and co-workers.

Acknowledgements

The research described here was funded by an EPSRC grant under the Applied Nonlinear Mathematics Initiative. The authors thank Tony Blakeborough, Allan McRobie and James Brownjohn for helpful discussion concerning engineering aspects of this problem. The authors are also grateful to Joe McKenna, Fabio Zanolin and Alessandro Fonda for sending and discussing reprints of their work in this problem area.

Appendix

We first give the formulae for the coefficients of the linear system (4.8-4.9) solved in order to determine $(1, n)$ -solutions. We first define some preliminary parameters. Subscripts on the parameters previously defined in (2.9) denote evaluation for \hat{y}_- and \hat{z}_- , and thus, for example, m is set to unity in those definitions.

$$s_\omega = \sin \sqrt{1 - \delta^2} \frac{2n\pi}{\omega}, \quad c_\omega = \cos \sqrt{1 - \delta^2} \frac{2n\pi}{\omega}, \quad (\text{A.1})$$

$$c_\Delta = \cos \sqrt{1 - \delta^2} \Delta t, \quad s_\Delta = \sin \sqrt{1 - \delta^2} \Delta t, \quad (\text{A.2})$$

$$\theta = c_\Delta s_\omega - s_\Delta c_\omega, \quad \phi = c_\Delta c_\omega + s_\Delta s_\omega, \quad (\text{A.3})$$

$$\tilde{A} = e^{\delta t} e^{-2n\pi\delta/\omega} \left(\phi - \frac{\delta\theta}{\sqrt{1-\delta^2}} \right), \quad \tilde{B} = e^{-\delta t} \left(c_m - \frac{\delta s_m}{\sqrt{m-\delta^2}} \right), \quad (\text{A.4})$$

$$\mu = (1 - \tilde{B}\tilde{A})^{-1}. \quad (\text{A.5})$$

The required coefficients are as follows,

$$\mathcal{A} = \mu\omega e^{-\delta t} \left(\tilde{B}\gamma_1 - \gamma c_m + \frac{\beta s_m}{\sqrt{m-\delta^2}} \right) + \sqrt{1-\delta^2}\theta^{-1} e^{-\delta t} e^{2n\pi\delta/\omega} \chi_1, \quad (\text{A.6})$$

$$\mathcal{B} = \mu e^{-\delta t} \left(\omega(-\tilde{B}\chi_1 + \chi c_m) + \frac{\lambda s_m}{\sqrt{m-\delta^2}} \right) + \sqrt{1-\delta^2}\theta^{-1} e^{-\delta t} e^{2n\pi\delta/\omega} \gamma_1, \quad (\text{A.7})$$

$$\mathcal{C} = \mu\omega \left\{ \tilde{B}e^{\delta t} e^{-2n\pi\delta/\omega} \left(\gamma_1\phi + \frac{\beta_1\theta}{\sqrt{1-\delta^2}} \right) - \gamma \right\} + \alpha_1 + \sqrt{1-\delta^2}\theta^{-1} \chi_1\phi, \quad (\text{A.8})$$

$$\mathcal{D} = \mu \left\{ \tilde{B}e^{\delta t} e^{-2n\pi\delta/\omega} \left(\omega\chi_1\phi + \frac{\lambda_1\theta}{\sqrt{1-\delta^2}} \right) - \omega\chi \right\} - \beta_1 + \sqrt{1-\delta^2}\theta^{-1} \gamma_1\phi, \quad (\text{A.9})$$

$$\Xi = -\mu \left(\frac{\tilde{B}e^{\delta t} e^{-2n\pi\delta/\omega} \theta}{\sqrt{1-\delta^2}} + \frac{e^{-\delta t} s_m}{\sqrt{m-\delta^2}} \right) + \delta + \sqrt{1-\delta^2}\theta^{-1} \left(\phi - e^{-\delta t} e^{2n\pi\delta/\omega} \right), \quad (\text{A.10})$$

$$\mathcal{E} = \mu\omega \left\{ \tilde{A}e^{-\delta t} \left(-\gamma c_m + \frac{\beta s_m}{\sqrt{m-\delta^2}} \right) + \gamma_1 \right\} - \alpha - \sqrt{m-\delta^2} \chi \frac{c_m}{s_m}, \quad (\text{A.11})$$

$$\mathcal{F} = \mu \left\{ \tilde{A}e^{-\delta t} \left(-\omega\chi c_m + \frac{\lambda s_m}{\sqrt{m-\delta^2}} \right) - \omega\chi_1 \right\} + \beta - \sqrt{m-\delta^2} \gamma \frac{c_m}{s_m}, \quad (\text{A.12})$$

$$\mathcal{G} = -\mu\omega \left\{ \tilde{A}\gamma + e^{\delta t} e^{-2n\pi\delta/\omega} \left(-\phi\gamma_1 + \frac{\beta_1\theta}{\sqrt{1-\delta^2}} \right) \right\} - \sqrt{m-\delta^2} \chi \frac{e^{\delta t}}{s_m}, \quad (\text{A.13})$$

$$\mathcal{H} = -\mu \left\{ -\omega\chi\tilde{A} + e^{\delta t} e^{-2n\pi\delta/\omega} \left(\omega\phi\chi_1 + \frac{\lambda_1\theta}{\sqrt{1-\delta^2}} \right) \right\} - \sqrt{m-\delta^2} \gamma \frac{e^{\delta t}}{s_m}, \quad (\text{A.14})$$

$$\Theta = -\mu \left(\frac{\tilde{A}e^{-\delta t} s_m}{\sqrt{m-\delta^2}} + \frac{e^{\delta t} e^{-2n\pi\delta/\omega} \theta}{\sqrt{1-\delta^2}} \right) + \frac{\delta}{m} - \frac{\sqrt{m-\delta^2}}{m} \left(c_m - \frac{e^{\delta t}}{s_m} \right). \quad (\text{A.15})$$

We now give the coefficients of the Jacobian stability matrix (5.3-5.4) for (1,n) orbits. We obtain

$$\frac{\partial f}{\partial t_o} = \left(\frac{e^{-\delta\Delta t}}{\hat{z}_+(t_1)} \right) \left(z_o c_m + \frac{s_m}{\sqrt{m-\delta^2}} (1 + F s_o - \delta z_o) \right) \quad (\text{A.16})$$

$$\frac{\partial f}{\partial z_o} = - \left(\frac{1}{\hat{z}_+(t_1)} \right) \frac{s_m e^{-\delta\Delta t}}{\sqrt{m-\delta^2}}, \quad (\text{A.17})$$

$$\begin{aligned} \frac{\partial g}{\partial t_0} = & \left(\frac{e^{-\delta\Delta t}}{\hat{z}_+(t_1)} \right) \left(z_o \left\{ (F - m\gamma) - m\chi c_1 c_m + \frac{s_m}{\sqrt{m-\delta^2}} (m\alpha c_1 - (m\beta + \delta F)s_1) \right\} \right. \\ & + \omega(1 + F s_o) \left\{ (\chi s_1 - \gamma c_1) c_m - \frac{s_m}{\sqrt{m-\delta^2}} (\alpha s_1 + \beta c_1) \right\} \\ & \left. e^{-\delta\Delta t} \{ z_o((m\gamma - F)s_o + m\chi c_o) - \omega(1 + F s_o)(\chi s_o - \gamma c_o) \} \right) \end{aligned} \quad (\text{A.18})$$

$$\begin{aligned} \frac{\partial g}{\partial z_o} = & \left(\frac{e^{-\delta\Delta t}}{\hat{z}_+(t_1)} \right) \left(\omega(\gamma c_1 - \chi s_1) + \frac{s_m}{\sqrt{m-\delta^2}} (\omega\beta c_1 + s_1(\lambda - F)) \right. \\ & \left. + e^{-\delta\Delta t} (z_o + \omega(\chi s_o - \gamma c_o)) \right) \end{aligned} \quad (\text{A.19})$$

where

$$c_m = \cos \sqrt{m - \delta^2} \Delta t, \quad s_m = \sin \sqrt{m - \delta^2} \Delta t. \quad (\text{A.20})$$

References

- Billah, K. Y. & Scanlan, R. H. (1991), ‘Resonance, Tacoma Narrows Bridge failure, and undergraduate physics textbooks’, *Am. J. Phys.* **59**(2), 118–124.
- Bishop, S. R. (1994), ‘Impact oscillators’, *Phil. Trans. Roy. Soc. Lond A* **347**, 347–351.
- Bleich, F., McCullough, C. B., Rosecrans, R. & Vincent, G. S. (1950), *The Mathematical Theory of Vibration in Suspension Bridges: A Contribution to the Work of the Advisory Board on the Investigation of Suspension Bridges*, Department of Commerce, Bureau of Public Roads, U. S. G. P. O., Washington.
- Brownjohn, J. M. W. (1994), Observations on non-linear dynamic characteristics of suspension bridges, Preprint. To appear in Earthquake Engrg. Struct. Dyn. 23.
- Budd, C. (1993), Grazing in impact oscillators, Preprint. To appear in Proceedings of the 1993 NATO Summer School on Complex Dynamical Systems.
- Budd, C. & Dux, F. (1994), ‘Chattering and related behaviour in impact oscillators’, *Phil. Trans. Roy. Soc. Lond A* **347**, 365–389.
- Budd, C., Dux, F. & Cliffe, A. (1993), The effect of frequency and clearance variations on single degree of freedom impact oscillators, Mathematics Research Report No. AM-93-02, Dept. of Mathematics, University of Bristol, University Walk, Bristol BS8 1TW, U. K.
- Choi, Q. H. & Jung, T. (1991), ‘On periodic solutions of the nonlinear suspension bridge equation’, *Diff. Int. Eqns* **4**(2), 383–396.
- Choi, Q. H., Jung, T. & McKenna, P. J. (1993), ‘The study of a nonlinear suspension bridge equation by a variational reduction method’, *Applicable Analysis* **50**, 73–92.
- Choi, Y. S., Jen, K. C. & McKenna, P. J. (1991), ‘The structure of the solution set for periodic oscillations in a suspension bridge model’, *IMA J. Appl. Math.* **47**, 283–306.
- Doedel, E. & Kerneves, J. P. (1986), AUTO: Software for continuation and bifurcation problems in ordinary differential equations, Applied mathematics report, California Institute of Technology, Pasadena.
- Elvey, J. S. N. (1983), ‘On the elimination of destabilizing motions of articulated mooring towers under steady sea conditions’, *IMA J. Appl. Math.* **31**, 235–252.
- Farquharson, F. B. (1950), *Aerodynamic Stability of Suspension Bridges with special reference to the Tacoma Narrows Bridge: Part I. Investigation Prior to October, 1941*, University of Washington Press, Seattle.

- Foale, S. & Bishop, S. R. (1992), ‘Dynamical complexities of forced impacting systems’, *Phil. Trans. Roy. Soc. Lond A* **338**, 547–556.
- Fonda, A. & Ramos, M. (1991), Large-amplitude subharmonic oscillations for scalar second order differential equations with asymmetric nonlinearities, Séminaire Mathématique, Rapport No. 195, Institut de Mathématique Pure et Appliquée, Université Catholique de Louvain, Bâtiment Marc de Hemptinne, Chemin du Cyclotron 2, 1348 Louvain-la-Neuve, Belgium. To appear J. Diff. Eqns.
- Fonda, A., Schneider, Z. & Zanolin, F. (1992), Periodic oscillations for a nonlinear suspension bridge model, Recherches de mathématique No. 18, Institut de Mathématique Pure et Appliquée, Université Catholique de Louvain, Bâtiment Marc de Hemptinne, Chemin du Cyclotron 2, 1348 Louvain-la-Neuve, Belgium. To appear J. Comp. Appl. Math.
- Glover, J., Lazer, A. C. & McKenna, P. J. (1989), ‘Existence and stability of large scale nonlinear oscillations in suspension bridges’, *ZAMP* **40**, 172–200.
- Guckenheimer, J. & Holmes, P. (1986), *Nonlinear Oscillations, Dynamical Systems, and Bifurcations of Vector Fields*, Vol. 42 of *Applied Mathematical Sciences*, Revised edn, Springer-Verlag, New York.
- Hogan, S. J. (1989), ‘On the dynamics of rigid-block motion under harmonic forcing’, *Proc. Roy. Soc. Lond. A* **425**, 441–476.
- Hogan, S. J. (1990), ‘The many steady state responses of a rigid block under harmonic forcing’, *Earthquake Engrg. Struct. Dyn.* **19**, 1057–1071.
- Hogan, S. J. (1992*a*), ‘The effect of damping on rigid block motion under harmonic forcing’, *Proc. Roy. Soc. Lond. A* **437**, 97–108.
- Hogan, S. J. (1992*b*), ‘Heteroclinic bifurcations in damped rigid block motion’, *Proc. Roy. Soc. Lond. A* **439**, 155–162.
- Hogan, S. J. (1994), ‘Slender rigid block motion’, *J. Eng. Mech. ASCE* **120**(1), 11–24.
- Jacover, D. & McKenna, P. J. (1994), ‘Nonlinear torsional flexings in a periodically forced suspended beam’, *J. of Comp. and Applied Math.* **52**, 241–265.
- Lazer, A. C. & McKenna, P. J. (1987), ‘Large scale oscillatory behaviour in loaded asymmetric systems’, *Ann. Inst. Henri Poincaré: Analyse non linéaire* **4**(3), 243–274.
- Lazer, A. C. & McKenna, P. J. (1990), ‘Large-amplitude periodic oscillations in suspension bridges: Some new connection with nonlinear analysis’, *SIAM Review* **32**(4), 537–578.
- Lazer, A. C. & McKenna, P. J. (1991), ‘Nonlinear flexings in a periodically forced floating beam’, *Math. Meth. Appl. Sci.* **14**, 1–33.
- McKenna, P. J. (1992), ‘Letters to the editor: Let’s twist again’, *American Scientist* **80**(1), 3–4.

- Nordmark, A. B. (1991), ‘Non-periodic motion caused by grazing incidence in an impact oscillator’, *J. Sound Vib.* **145**(2), 279–297.
- Nordmark, A. B. (1992), ‘Effects due to low velocity impact in mechanical oscillators’, *Int. J. Bifn. Chaos* **2**(3), 597–605.
- Ostenfeld, K. H. & Larsen, A. (1992), Bridge engineering and aerodynamics, in ‘Proceedings of the First International Conference on Aerodynamics of Large Bridges, 19-21 February 1992, Copenhagen, Denmark’, A. A. Balkema, Rotterdam, pp. 3–22.
- Peterson, I. (1990), ‘Rock and roll bridge’, *Science News* **137**, 344–346.
- Petroski, H. (1991), ‘Engineering: Still twisting’, *American Scientist* **79**(5), 398–401.
- Shaw, S. W. (1985*a*), ‘The dynamics of a harmonically excited system having rigid amplitude constraints. part i: Subharmonic motions and local bifurcations.’, *ASME J. Appl. Mech.* **52**, 453–458.
- Shaw, S. W. (1985*b*), ‘The dynamics of a harmonically excited system having rigid amplitude constraints. part ii: Chaotic motions and global bifurcations.’, *ASME J. Appl. Mech.* **52**, 459–464.
- Shaw, S. W. & Holmes, P. J. (1983), ‘A periodically forced piecewise linear oscillator’, *J. Sound Vib.* **90**(1), 129–155.
- Stensson, A. & Nordmark, A. B. (1994), ‘Experimental investigation of some consequences of low velocity impacts in the chaotic dynamics of a mechanical system’, *Phil. Trans. Roy. Soc. Lond A* **347**, 439–448.
- Thompson, J. M. T., Bokian, A. R. & Ghaffari, R. (1983), ‘Subharmonic resonances and chaotic motions of a bilinear oscillator’, *IMA J. Appl. Math.* **31**, 207–234.
- Thomson, W. T. (1993), *Theory of Vibration with Applications*, Fourth edn, Prentice Hall, New York.
- Timoshenko, S. (1928), *Vibration Problems in Engineering*, Constable and Company Ltd., London.
- Whiston, G. S. (1987*a*), ‘Global dynamics of a vibro-impacting linear oscillator’, *J. Sound Vib.* **118**, 395–429.
- Whiston, G. S. (1987*b*), ‘The vibro-impact response of a harmonically excited and preloaded one-dimensional linear oscillator’, *J. Sound Vib.* **115**(2), 303–319.
- Whiston, G. S. (1992), ‘Singularities in vibro-impact dynamics’, *J. Sound Vib.* **152**(3), 427–460.